SCIENTIFIC REP⚙RTS

Antibiotic binding of STY3178, a yfdX protein from *Salmonella* Typhi

Paramita Saha[1], Camelia Manna[1], Santasabuj Das[2] & Mahua Ghosh[1]

The yfdX family proteins are known for long time to occur in various virulent bacteria including their multidrug resistant (MDR) strains, without any direct assigned function for them. However, yfdX protein along with other proteins involved in acid tolerance response is reported to be up regulated by the multidrug response regulatory system in *E. coli*. Hence, molecular and functional characterization of this protein is important for understanding of key cellular processes in bacterial cells. Here we study STY3178, a yfdX protein from a MDR strain of typhoid fever causing *Salmonella* Typhi. Our experimental results indicate that STY3178 is a helical protein existing in a trimeric oligomerization state in solution. We also observe many small antibiotics, like ciprofloxacin, rifampin and ampicillin viably interact with this protein. The dissociation constants from the quenching of steady state fluorescence and isothermal titration calorimetry show that ciprofloxacin binding is stronger than rifampin followed by ampicillin.

Bacteria are one of the major sources for human infections. The bacterial proteins leading to virulence are of fundamental significance. Many of these bacterial proteins have no functional annotation and are termed as domains of unknown function (DUF)[1]. Availability of complete genome sequence for many bacterial strains increases the number of identified DUF proteins whose functional characterization remains grossly incomplete.

Among the DUF proteins, the yfdX protein family is a prominent member. These yfdX proteins have orthologues identified in many virulent bacteria, such as *E. coli, S. Typhi, S. Typhimurium, S. Paratyphi, K. pneumoniae, P. ananatis, E. tarda, H. alvei* and *P. shigelloides*[2-11]. Many of the strains of these virulent bacteria are also multidrug resistant (MDR). yfdX protein is first identified in *E. coli*[12,13] where the expression of multidrug response regulator protein evgA induced the co-expression of yfdX protein in the cytoplasmic fraction. DNA microarray analysis has further shown that expression of a group of proteins, yfdW, yfdU yfdV, yfdE and yfdX are up regulated by evgA. A significant (orders of magnitude) enhancement of the expression for yfdX gene was observed[13,14] compared to other yfdWUVE proteins upon overproduction of evgA in *E. coli* when quantified using real time PCR. Proteins yfdWUVE are primarily involved in acid tolerance response (ATR) activity[15]. However, yfdX proteins till date remain completely uncharacterized to the best of our knowledge. Occurrence of yfdX proteins in disease-causing bacteria and its co-expression along with the multidrug response regulator protein in *E. coli* indicates that this protein probably has functional role in bacteria which is hitherto unknown. Structure of a yfdX protein from *K. pneumoniae* is reported till date in the protein data bank (PDB 3DZA) which is a tetramer containing metal ions in the monomer interfaces. No functional characterization is reported for this protein as well.

STY3178 is a yfdX protein from the MDR strain (CT18) of *Salmonella* Typhi, the etiologic agent of a potentially lethal febrile illness in the humans[3]. Typhoid fever is a major public health threat to the developing countries worldwide and the concern has significantly increased with the prevalence of MDR strains. *S*. Typhi (CT18) is reported to be resistant[16-20] to many antibiotics like ciprofloxacin (Cpx), rifampin (Rfp), ampicillin (Amp) and so on. The homologues of STY3178 are found across almost all the species of *Salmonella* genus. According to the different database predictions STY3178 is predicted either as a putative membrane protein (Topsan[21]) or as a periplasmic protein (Uniprot[22] and NCBI). The Kegg[23] and STRING[24] databases even mention STY3178 as a completely hypothetical protein.

In the present study we characterize STY3178 protein biophysically and show its interaction with different antibiotic molecules. The questions of our interest are the following: (i) Is STY3178 an oligomeric protein in solution given that its orthologue from *K. pneumoniae* has a tetrameric structure as reported? (ii) Is STY3178 capable of binding drugs or antibiotic molecules? In solution we find STY3178 is a well-folded primarily α-helical protein like its orthologue. Dynamic light scattering (DLS), size exclusion chromatography (SEC) and nuclear

[1]Department of Chemical, Biological And Macromolecular Sciences, S. N. Bose National Centre for Basic Sciences, Block JD, Sector III, Salt lake, Kolkata 700098, India. [2]Division of Clinical Medicine, National Institute of Cholera and Enteric Diseases, P-33, C.I.T. Road, Scheme XM Beleghata, Kolkata 700 010, India. Correspondence and requests for materials should be addressed to M.G. (email: mahuaghosh@bose.res.in or mahua.ghosh@gmail.com)
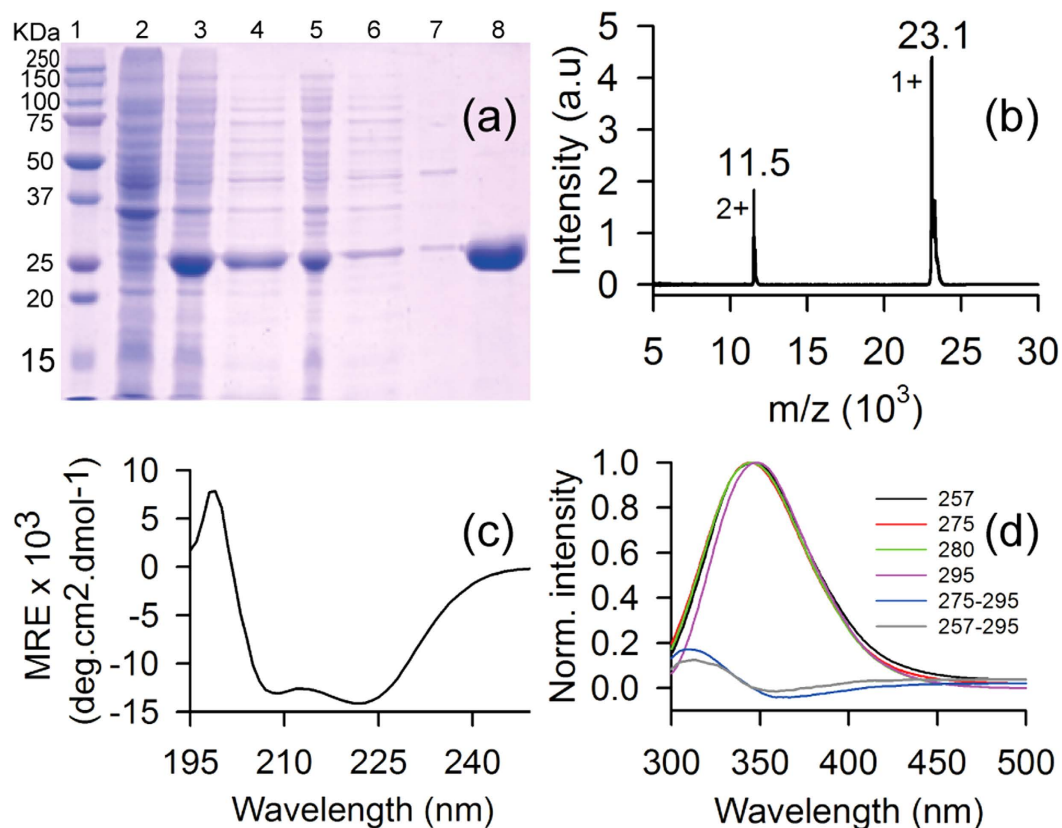
**Figure 1. Overexpression, purification, and preliminary characterization of the protein STY3178.** (**a**) SDS-PAGE showing the molecular weight marker in lane 1; un-induced cells, lane 2; induced cells, lane 3; crude extract of soluble protein, lane 4; insoluble cell debris, lane 5; flow through from Ni-NTA affinity column, lane 6; wash from Ni-NTA affinity column, lane 7; elute from affinity column, lane 8. (**b**) MALDI-TOF mass spectrum of the purified protein showing peak at 23.1 KDa for the singly charged species. (**c**) Far UV-CD spectrum of the pure protein showing α-helical secondary structure with two characteristic minima around 209 nm and 222 nm. (**d**) Steady state fluorescence emission spectra of the protein for excitation wavelengths 257 (black), 275 nm (red), 280 (green) and 295 nm (magenta). The difference fluorescence spectra (275–295 nm) and (257–295) showing FRET intensity is shown in blue and grey, respectively.

magnetic resonance (NMR) relaxation measurements indicate that STY3178 is a trimer. We investigate antibiotic interaction with STY3178 for three different antibiotics to which *S.* Typhi (CT18) is resistant. Finally we quantify the respective binding parameters of these antibiotics to protein and find them in the biologically relevant regime. Our data indicate that ciprofloxacin (Cpx) binds to the protein with higher affinity than rifampin (Rfp) and ampicillin (Amp) binding is weakest among the three.

Results

Cloning of our gene of interest (*sty3178)* in prokaryotic expression plasmid pET28a is confirmed by sequencing. Recombinant 6-His-tagged protein (without the N-terminal signal peptide) is expressed successfully in *E. coli* which migrates in SDS-PAGE around ~25 KDa as shown in Fig. 1a (lane 3). High purity of protein is obtained after single step purification as judged from the SDS-PAGE and Coomassie staining (Fig. 1a, lane 8). The calculated molecular weight of the construct is ~23.11 KDa whereas the purified protein migrate around 25 KDa in SDS-PAGE (Fig. 1a, lane 8). We perform mass spectrometry of the purified protein to confirm the actual molecular mass using MALDI-TOF. Figure 1b shows the mass spectrum of the purified protein where the m/z ratio indicates the molecular mass ~23.1 KDa for STY3178. The other peak at 11.5 KDa is assigned for the doubly charged species of the same protein. STY3178 is predicted by Topsan[21] database as a putative membrane protein, however, we find it in the soluble fraction as observed in the SDS-PAGE (Fig. 1a, lanes 4 and 8). This observation is in complete agreement with the earlier study from *E. coli*[12] where the orthologues yfdX protein is expressed in the cytoplasm.

The far UV-CD spectrum of purified STY3178 confirms the presence of a well folded protein in solution (Fig. 1c). The spectrum reveals typical characteristic of an α-helix containing protein with two minima at 209 nm and 222 nm, respectively. The estimated[25,26] helix content of the protein using the ellipticity value at 222 nm is ~44%. The ellipticity of the entire complete CD spectrum is further used in Dichroweb server[27–29] following the K2D[30] method, we find ~50% helix and ~20% β-sheet content for the protein.
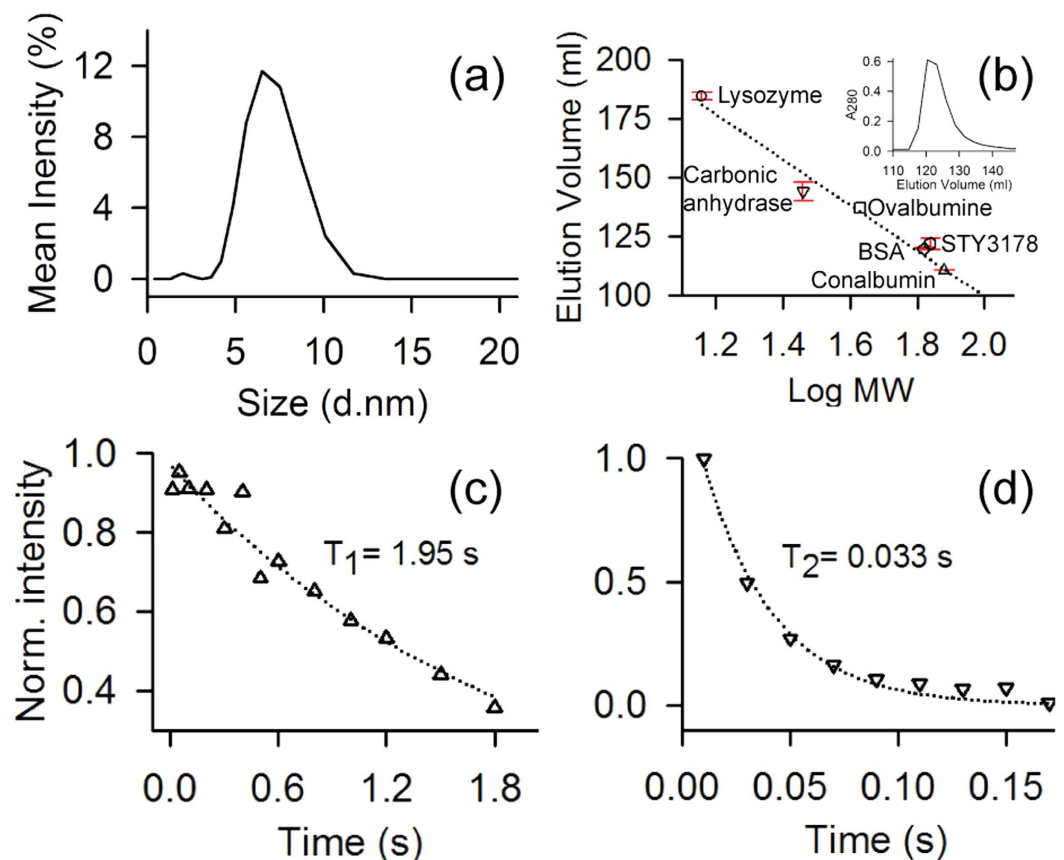
Figure 2. Aggregation state and NMR relaxation measurement for protein STY3178. (a) DLS spectrum of the protein showing maximum scattering intensity around a hydrodynamic diameter of 6.5 nm. (**b**) The elution volume versus logarithm of molecular weight of protein in the superdex75 column showing data for lysozyme (14.4 KDa, circle); carbonic anhydrase (29 KDa, inverted triangle); ovalbumin (43 KDa, square); BSA (66 KDa, diamond); STY3178 (hexagon) and Conalbumin (75 KDa, triangle). The error bars are the standard errors estimated using the average elution volume for the repeated experiments. The inset shows the corresponding size exclusion chromatogram for STY3178. (**c**) and (**d**) Show T_1 and T_2 relaxation values acquired for the uniformly ^{15}N-labelled STY3178 protein, respectively. The delay times used for T_1 measurements are 0.01, 0.05, 0.1, 0.2, 0.3, 0.4, 0.5, 0.6, 0.8, 1.0, 1.2, 1.5, 1.8 s and for T_2 measurements are 0.01, 0.03, 0.05, 0.07, 0.09, 0.11, 0.13, 0.15, 0.17 s. The corresponding T_1 and T_2 values are extracted by fitting the single exponential decay equation.

The steady state fluorescence emission spectrum of STY3178 at 20 °C indicates the emission peak position commensurate to Trp emission for any of the following excitation wavelengths 257 nm (black), 275 nm (red), 280 nm (green) or 295 nm (magenta) as shown in Fig. 1d. There are two Phe and five Tyr residues in the protein, but the fluorescence emission from 257 nm and 275 nm excitations are similar to the reported Trp emissions. This indicates a possibility of FÖrster resonance energy transfer (FRET) between Tyr-Trp and Phe-Trp pairs. Difference spectra of 275–295 nm and 257–295 nm excitation wavelengths confirm the signature of FRET between Tyr-Trp (Fig. 1d, blue) and Phe-Trp (Fig. 1d, grey) pairs, respectively. The intensity of FRET is lower for excitation 257–295 compared to 275–295 excitation. At 257 nm excitation all the three aromatic residues could get excited. Phe has a lower quantum yield compared to Tyr or Trp. In addition, Phe emits around 280 nm which is the absorption wavelength for Tyr and Trp resulting in lower intensity of FRET between Phe and Trp (Fig. 1d, grey).

State of aggregation of the protein. Figure 2a shows the average hydrodynamic diameter of the protein in solution ~6.5 nm as observed using dynamic light scattering (DLS). The measured hydrodynamic size is much higher compared to a 23 KDa protein as per the relationship between hydrodynamic size and molecular weight (MW) of different standard globular proteins[31]. For instance, proteins like soyabean trypsin inhibitor (20 KDa) and carbonic anhydrase (29 KDa) have hydrodynamic radius ~2.4 nm and that of ovalbumin (45 KDa) is 2.8 nm as reported earlier[32,33]. Thus, a hydrodynamic radius of 3.25 nm for STY3178 would correspond to MW higher than 50 KDa.

The DLS data clearly indicates a size anomaly for the protein in solution considering it as a monomer. To address this anomaly we perform size exclusion chromatography for STY3178 using Superdex75 column (GE healthcare). The elution profile of STY3178 from the column (inset shown in Fig. 2b) is compared with many standard proteins in the molecular weight range of 14 KDa to 75 KDa (Fig. 2b). We find that all these proteins

elute from the column at similar volumes repeatedly as indicated by the small error bars in Fig. 2b. STY3178 elutes in the molecular weight regime similar to 66 KDa. This indicates that STY3178 forms a trimer in solution.

We calculate the rotational correlation time (τ_C) using Stokes-Einstein-Debye (SED) equation $\tau_C = 4\pi\eta R^3/3KT$ (where η and R are the viscosity and hydrodynamic radius, respectively) for our measured hydrodynamic radius. Using this relationship we obtain τ_C value ~30.5 ns. This τ_C is again much higher compared to protein of similar molecular weight like α-chymotrypsin (25 KDa) where the reported τ_C is about 13.4 ns[34].

We estimate τ_C of STY3178 using NMR spectroscopy by acquiring one dimensional (1D) ^{1}H-^{15}N heteronuclear longitudinal (T_1) and transverse (T_2) relaxation data. Since the T_1 relaxation times are typically longer than T_2 relaxation times we perform the T_1 measurement for three different d_1 delays and average the normalized peak intensities over these measurements. Figure 2c,d show the average peak intensities in 8.5–10.5 ppm region of the spectra plotted against the corresponding delay times in the T_1 and T_2 experiments, respectively. The T_1 and T_2 values are extracted from the exponential fit of the decays of the integrated peak intensity. We find T_1 and T_2 values ~1.95 s and ~0.033 s respectively. The rotational correlation time τ_C calculated using the experimentally observed T_1 and T_2 (as described in methods) is ~24.7 ns. This estimated rotational correlation time is in reasonable agreement with the calculated τ_C from hydrodynamic radius using the SED equation. Thus all our experimental results indicate a trimeric state of oligomerization for the protein in solution.
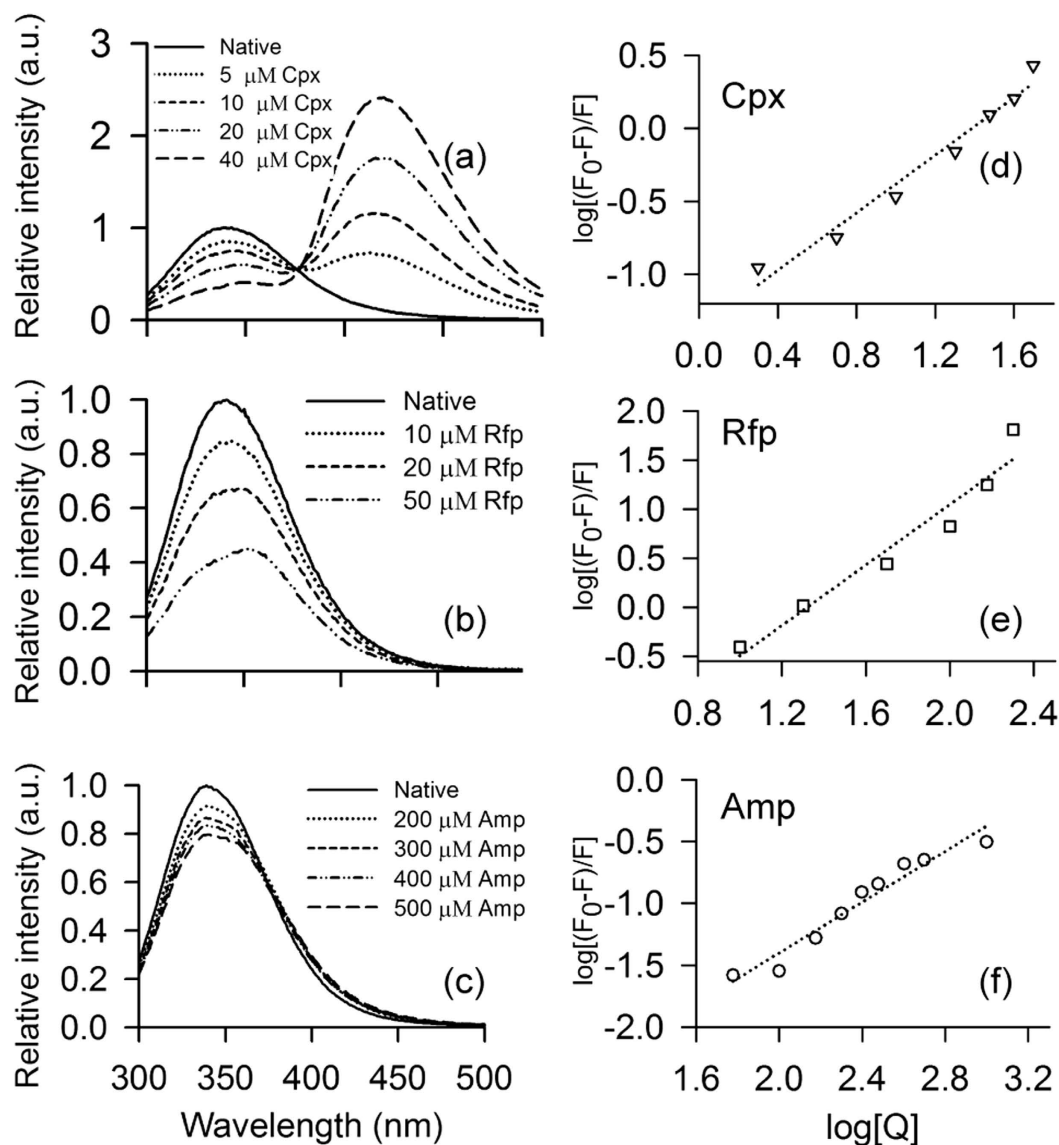
Antibiotic interaction of STY3178.

We probe small antibiotic interactions for STY3178 with three different antibiotics, namely, ciprofloxacin (Cpx), rifampin (Rfp) and ampicillin (Amp) using steady state fluorescence spectroscopy, isothermal titration calorimetry (ITC) and circular dichroism. The CT18 strain[3,5] of *S.* Typhi is reported to be resistant to these antibiotics[16–20]. We observe fluorescence emission of the protein in presence of antibiotics is quenched considerably compared to the native spectra. A shift in emission peak position for Cpx and Rfp binding (Fig. 3a,b) is observed which is negligible for Amp binding (Fig. 3c). The amount of quenching is, however, different for different antibiotics (Fig.3a–c). We monitor the change in fluorescence intensity with increasing concentration of the antibiotics (Q) for 280 nm excitation wavelength. The fluorescence quenching constant K_{SV} is measured using Stern-Volmer equation[35–37] as described in methods. The value of quenching constant (Table 1) is found different for the three antibiotics. We then measure the binding constant (K) for each antibiotic using the modified form of Stern-Volmer equation[35–37] (see methods). Figure 3d–f show the plots of $\log[(F_0 - F)/F]$ versus $\log[Q]$ for the three antibiotics Cpx, Rfp and Amp, respectively. The intercept of the fitted curve provides the value for K and the slopes provide the information on the number of binding sites (n) as summarised in Table 1. Fluorescence data indicate Cpx and Amp bind to a single site (n≈1). However, Rfp has a possibility of binding in more than one site with n (≈1.5) exceeding unity. The dissociation constant (K_d) is calculated from the reciprocal of K (Table 1). We estimate the ΔG for each of these protein-antibiotic interactions from the K values and summarise them in Table 1.

We verify these antibiotic interactions using ITC. The thermograms for Cpx, Rfp and Amp recorded at 298 K are shown in Fig. 4a–c and the corresponding binding isotherms in Fig. 4d–f, respectively. We fit the isotherms in a sequential binding model for Cpx and Amp whereas Rfp data is fitted to a single site model. The binding parameters, including K, K_d, enthalpy changes (ΔH), ΔG and entropy changes ($T\Delta S$) are detailed in Table 2. In the sequential binding model fits, we have considered only the stronger binding parameters. The ITC data indicate binding of Cpx, Rfp and Amp with STY3178 where the dissociation constants belong to the micro molar (μM) range. We observe that Cpx binds stronger than Rfp and Amp. ΔG of Cpx binding is more favourable followed by Rfp and Amp. This trend of binding constants and the ΔG from ITC are similar to those from steady state fluorescence measurements, although the ITC data show much stronger binding.

We probe the structural changes induced in the protein in presence of antibiotics using CD. The near UV-CD spectra of the protein in antibiotic free and bound states are shown in Fig. 5a–c. The native protein structure shows a broad peak around 250–280 nm. This broad peak indicates the involvement of aromatic residues in the tertiary structure of the protein[38]. We observe changes in this broad peak structure in presence of antibiotics. However, the extent of changes is different for different antibiotics and sensitive to their concentrations. For instance, in presence of ciprofloxacin with increasing concentration, two peaks start appearing near ~260 nm and ~280 nm as shown in Fig. 5a. These peaks are similar to Phe and Tyr fine structures as reported in literature[26,38]. This indicates that ciprofloxacin interaction with the protein occurs near Phe and Tyr residues. Perturbation of aromatic residues upon addition of rifampin to the protein shows a similar trend like ciprofloxacin binding. The ellipticity values are different for binding with different concentration of ciprofloxacin (Fig. 5a) and rifampin (Fig. 5b) with the peak positions remaining similar. On the other hand, ampicillin binding to the protein (Fig. 5c) shows negligible change compared to the native spectrum.

The far UV-CD spectra in presence of all the three antibiotics are very similar to the native protein structure (Fig. 5d). A slight decrease in ellipticity is observed for rifampin and ampicillin bound protein whereas no substantial change is observed upon ciprofloxacin binding. The percentage of helix content for the native as well as antibiotic bound proteins are tabulated in Table 3 where we find only 3% decrease in helix content for rifampin and ampicillin bound structures when compared to the native. Thus the secondary structural elements remain largely unaffected by the antibiotics.

We further estimate the τ_c of the protein in presence of antibiotics to probe any change in the oligomeric state. Table 3 summarises the T_1, T_2 and τ_c values for the native and antibiotic bound protein. We find no noticeable change in the τ_c of the protein in bound state for all the antibiotics. This indicates that the aggregation state of the protein remains same upon binding these small ligands. This is further confirmed from the hydrodynamic radius (R_H) of the molecule which also remains unchanged for the antibiotic bound protein when measured using DLS as given in Table 3.
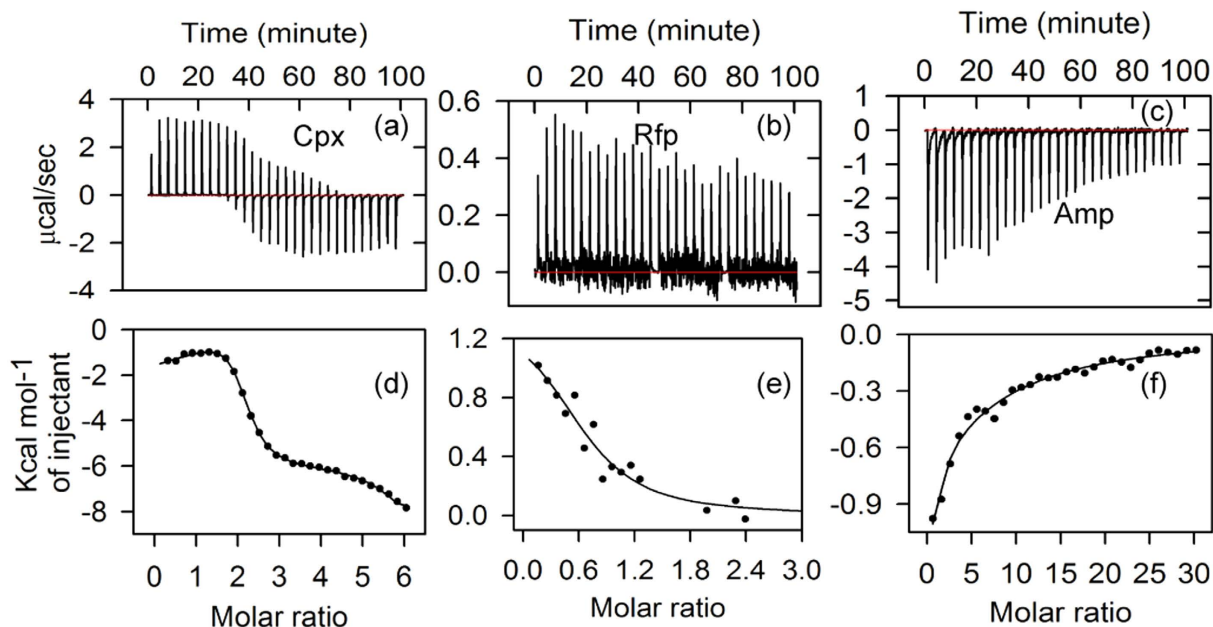
Figure 3. Interaction of STY3178 with antibiotics from fluorescence. (**a–c**) Show the fluorescence emission spectra of STY3178 in presence of different concentrations of ciprofloxacin (Cpx), rifampin (Rfp) and ampicillin (Amp), respectively, for excitation wavelength of 280 nm. (**d–f**) Show the plot of $\log[(F_0 - F)/F]$ against $\log[Q]$ for Cpx (inverted triangle), Rfp (square) and Amp (circle), respectively.

Antibiotic bound	K_{SV} (μM^{-1})	K (μM^{-1})	K_d (μM)	n	ΔG (KJ mol^{-1})
Cpx	0.05 ($\pm$ 0.002)	0.04 ($\pm$ 0.0023)	25.0 ($\pm$ 1.2)	0.99	−26.5
Rfp	0.26 ($\pm$ 0.034)	0.01 ($\pm$ 0.004)	100.0 ($\pm$ 20.5)	1.54	−22.8
Amp	0.0003 ($\pm$ 0.00002)	0.0004 ($\pm$ 0.00004)	2500.0 ($\pm$ 370.5)	1.03	−14.6

Table 1. STY3178-antibiotic interaction data from steady state fluorescence measurement.

Discussion

We find STY3178 is a well folded and predominantly α-helical protein containing some β-sheet elements. This observation is similar to the secondary structural elements of the orthologues protein structure 3DZA available in the PDB. Our experiments also suggest that STY3178 is an oligomer in solution similar to 3DZA. However, STY3178 is a trimer, whereas the 3DZA structure is as a tetramer. We rule out any possibility of stable tetrameric aggregation for STY3178 based on our experimental observations. STY3178 tetramer would be of MW 92 KDa, had it been a stable tetramer. When we compare the proteins of MW higher than 90 KDa we find the reported hydrodynamic radius for them to be larger than 3.25 nm (Supplementary Table S1). In the elution volume versus log MW plot of SEC data, STY3178 would be a mismatch point from the standard protein line not following the

Figure 4. STY3178 interaction with antibiotics from ITC. The thermogram of (**a**) ciprofloxacin (Cpx) bound STY3178, (**b**) rifampin (Rfp) bound and (**c**) Ampicillin (Amp) bound protein. Fitted isotherms are shown for interaction of (**d**) Cpx, (**e**) Rfp and (**f**) Amp with STY3178.

| Antibiotic bound	K (µM^{-1})	K_d (µM)	ΔH (KJ mol^{-1})	$T\Delta S$ (KJ mol^{-1})	ΔG (KJ mol^{-1})
Cpx	$K_1 = 0.58$ (± 0.04)	$K_{d1} = 1.72$	$\Delta H_1 = -6.49$ (± 0.55)	$T\Delta S_1 = 26.53$	$\Delta G_1 = -33.02$
	$K_2 = 0.423$ (± 0.0079)	$K_{d2} = 2.36$	$\Delta H_2 = -4.03$ (± 1.13)	$T\Delta S_2 = 28.16$	$\Delta G_2 = -32.19$
Rfp	$K_1 = 0.0151$ (± 0.00911)	$K_{d1} = 66.23$	$\Delta H_1 = 6.00$ (± 1.62)	$T\Delta S_1 = 29.91$	$\Delta G_1 = -23.91$
Amp	$K_1 = 0.00744$ (± 0.0037)	$K_{d1} = 134.41$	$\Delta H_1 = -6.54$ (± 1.07)	$T\Delta S_1 = 15.65$	$\Delta G_1 = -22.19$

Table 2. STY3178-antibiotic binding parameters from ITC.

slope if the protein is a tetramer. These observations indicate that the yfdX proteins seem to have a propensity for oligomeric state formation but the degree of oligomerization varies within the family. This is a feature observed for other small oligomeric proteins like family of small heat shock proteins[39].

Our experimental data demonstrate that different small antibiotics are capable of binding to STY3178. Both steady state fluorescence and ITC results show binding preference towards Cpx, followed by Rfp and Amp. The K_d values for Cpx binding measured from ITC are an order of magnitude stronger than that measured from fluorescence. Similarly, Amp binding is captured well from ITC, whereas fluorescence data indicate much weaker binding. However, for Rfp binding, the K_d value is similar as obtained from both the measurements. The stoichiometries of binding from ITC and fluorescence results are not the same. These discrepancies may be due to the fact that fluorescence quenching depends on the binding of the antibiotics in the vicinity of the fluorophores, while ITC is independent of this. The binding modes for all these three antibiotics are different as suggested by different fitting protocols required for the isotherms.

These antibiotics neither perturb the secondary structure as observed from far UV-CD nor affect the oligomeric state of the protein as detected in DLS and NMR relaxation measurements. However, they show tertiary structural rearrangement as observed in the near UV-CD (Fig. 5a–c). The probable residues involved in the interaction are the aromatic residues of the protein. We study the near UV-CD of the isolated aromatic residues in presence of antibiotic molecules. All the three isolated amino acids Phe, Tyr and Trp in presence of Cpx show change in spectra (supplementary Fig. S1a). On the other hand, in presence of Rfp, the changes are small for isolated Phe but isolated Tyr and Trp show pronounced changes (supplementary Fig. S1b) qualitatively similar to that observed for protein. When we compare the nature of perturbation in presence of Amp (supplementary Fig. S1c), very little changes are seen for isolated Phe and Trp but the change in isolated Tyr is again qualitatively similar to the nature of change observed in protein (Fig. 5c).

The native protein fluorescence shows signature of FRET between the aromatic residues (Fig. 1d). In presence of antibiotics, this FRET signature changes (Fig. 5e,f). In Fig. 5e we find an enhancement of FRET upon Amp binding whereas decrease in FRET intensity for Cpx binding. FRET intensity does not change in Rfp bound
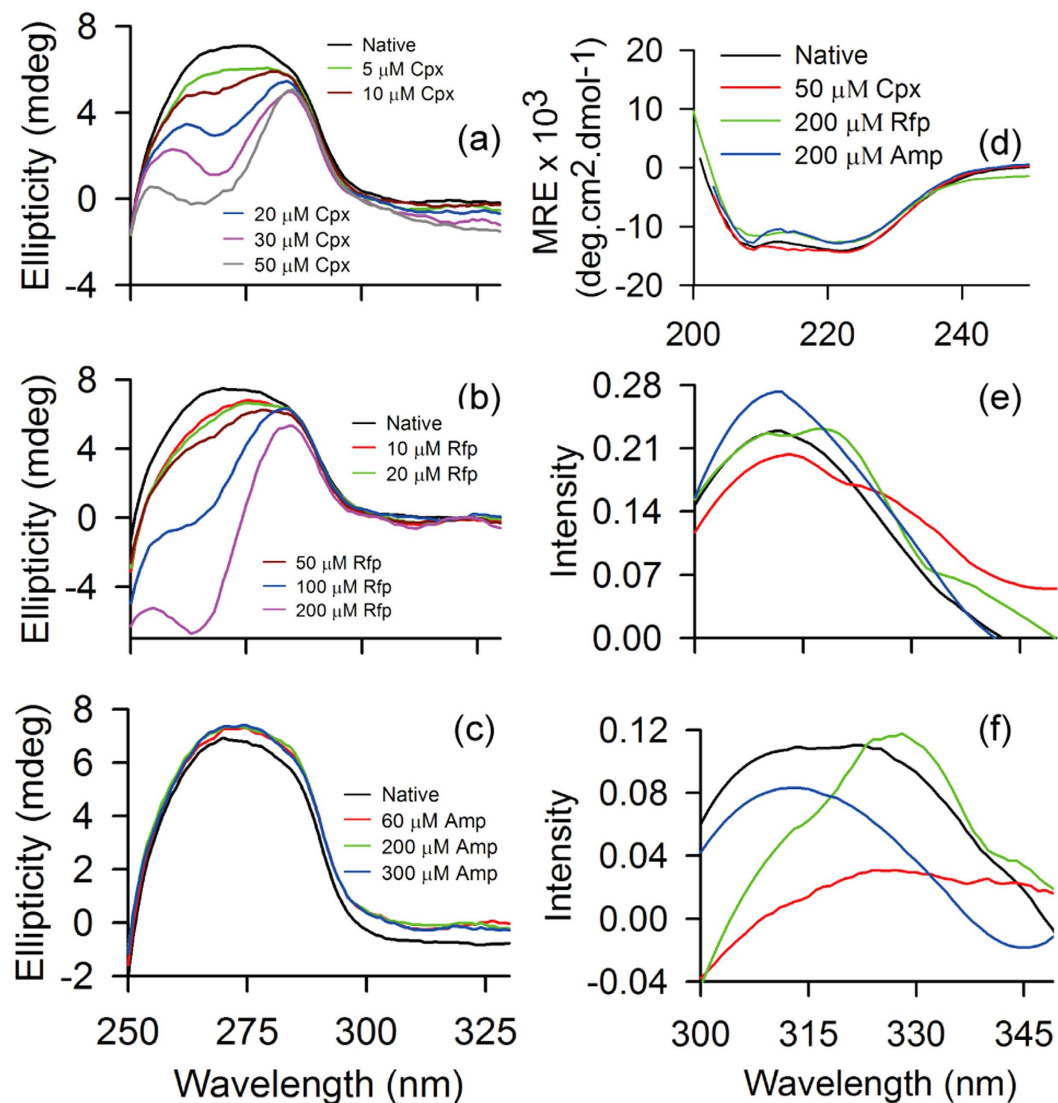
Figure 5. Antibiotic free and bound STY3178 CD spectra and fluorescence difference spectra. (a–c) Show the near UV-CD spectra in the range 250–330 nm. The different concentrations of (**a**) ciprofloxacin used are 5 μM (green), 10 μM (brown), 20 μM (blue), 30 μM (magenta) and 50 μM (grey); (**b**) rifampin are 10 μM (red), 20 μM (green), 50 μM (brown), 100 μM (blue), 200 μM (magenta) and (**c**) ampicillin are 60 μM (red), 200 μM (green) and 300 μM (blue). (**d**) Shows the far UV-CD (200 nm- 250 nm) spectra in antibiotic bound and free state. The difference fluorescence emission spectra are shown for (**e**) 275–295 nm and (f) 257–295 nm. The native protein is shown in black, ciprofloxacin (50 μM) bound protein in red, rifampin (200 μM) bound in green and ampicillin (200 μM) bound form in blue in panels (**d–f**).

State	Helix (%)	T_1 (s)	T_2 (s)	τ_c (ns)	R_H (nm)
Native protein	43.9	1.95	0.033	24.7	3.25
Protein bound with Cpx	44.5	1.98	0.036	23.8	3.25
Protein bound with Rfp	40.1	2.11	0.033	25.9	3.25
Protein bound with Amp	40.6	1.92	0.034	24.2	3.25

Table 3. Percentage of helix, longitudinal relaxation time (T_1), transverse relaxation time (T_2), calculated rotational correlation time (τ_c) and hydrodynamic radius (R_H) of native and antibiotic bound STY3178.

protein but the difference spectrum shows appearance of another peak different from the native peak ~318 nm having same intensity. In the difference spectra of 257–295 nm shown in Fig. 5f, we observe a decrease in intensity

of FRET upon Amp binding and a qualitative change of the overall spectrum in presence of Rfp showing a peak ~330 nm. The FRET signature of 257–295 nm is significantly quenched in presence of Cpx. These observations indicate that the aromatic residues involved in FRET are also associated with antibiotic binding.

Interestingly, we find that similar binding site interactions containing aromatic amino acids are observed in proteins associated with multidrug efflux process. For instance, in BmrR[40] bound to kanamycin or tetracycline, the antibiotic is stacked near Tyr and Phe residues. Similarly, Phe is found in the vicinity of Rfp in the antibiotic bound structure of AcrB[41]. Amp bound OmpF[42] has both Phe and Tyr in the near vicinity of the antibiotic. This observation is also seen for other small molecule binding like rhodamine 6G in RamR[43] where Phe participates in the interaction.

The binding parameters, K and K_d for nearly 100 different protein-antibiotic binding and protein-small molecule interactions[43–49] are tabulated in Supplementary Table S2. We observe K_d values lie in the range 1–100 μM for more than ~80% cases. The next ~15% belong to the range 100–200 μM and less than 5% in the range 200–300 μM. Our data from ITC fall in the lowest K_d range. Thus, STY3178 shows antibiotic binding capability in the biologically relevant regime.

The blast[50] search of STY3178 indicates that this yfdX protein is highly conserved among all *Salmonella* species with 92% or higher sequence identity. STY3178 also shares a minimum of 40% sequence similarity with other reported yfdX proteins from various bacteria. Sequence alignment of yfdX proteins from the MDR strains of several bacteria[2–11] are shown in supplementary Fig. S2. Such high sequence similarity from different organisms indicates that they might have similar structural fold. However, the order of oligomerization for different yfdX proteins can differ depending on the primary sequence and the size of the protein. The other notable feature that transpires from the sequence alignment is that several locations have conserved Tyr and Phe residues. For instance, we find in 3DZA structure one Phe and two consecutive Tyr residues are in close proximity and these residues are conserved as well. This indicates that 3DZA could be involved in antibiotic interaction like STY3178. Among the yfdX family protein these proximal Phe and consecutive Tyr residues of 3DZA are conserved as well indicating possibility of similar antibiotic interaction as observed for STY3178.

In conclusion, we have characterized the yfdX protein STY3178 from the MDR strain of *S.* Typhi and identified its antibiotic binding ability for the first time to the best of our knowledge. The oligomeric state of the protein in solution is revealed from the biophysical characterization using CD, fluorescence and NMR studies. Our study reveals that yfdX protein, even though not functionally characterized, may not be completely non-functional which in turn opens up further possible studies for this family of proteins. Such studies could be immensely helpful to understand their involvement in pathogenic activity of virulent bacteria.

Material And Methods

Cloning. The gene of interest (*sty3178*) with 573 base pair encoding the desired protein is amplified by polymerase chain reaction (PCR) from *S.* Typhi gemonic DNA. The forward and reverse primers used during this amplification are 5′-CATATGGCCGCAACAAACATGACTG-3′ and 5′- CTCGAGGATATTAATGCGCGGCGTCGTG -3′ (Integrated DNA Technologies), respectively. The primers contain the restriction sites for the enzymes NdeI (CATATG) and XhoI (CTCGAG). The amplified PCR product is then inserted into TA vector using T4 DNA ligase and transformed into Top10 *E.coli* cells (Novagen). The transformed bacteria with the desired gene are confirmed by screening the blue/white colonies followed by colony PCR. The plasmid prepared from the transformants is then digested and the insert is purified and sub-cloned into the pET28a expression vector (Novagen). The sub-cloning is confirmed using T7 sequencing primers specific for pET28a expression system. The plasmid containing the desired gene is transformed into *E.coli* BL21(DE3) strain (Novagen).

Overexpression. Transformed cells containing the plasmid pET28a with *sty3178* gene are grown in 5 ml Luria-Bertani (LB) medium overnight at 37 °C with constant shaking at 250 rpm in a shaker (Innova 42 New Brunswick Scientific). 1% of starter culture is used to inoculate 1 litre of fresh LB and the bacteria are grown till optical density (OD_{600}) reaches 0.9. Overexpression is induced by 0.2 mM isopropyl-β-D-thiogalactoside for 4hrs. The cells are then harvested by centrifugation (Eppendorf) at 5000 g for 10 minutes at 4 °C.

Purification. Harvested cells are resuspended in lysis buffer containing 50 mM potassium phosphate (pH 7), 250 mM sodium chloride (NaCl) and 1 mM phenylmethanesulfonyl fluoride (PMSF) and disrupted by sonication (Sartorius LABSONIC) at 30% amplitude and 0.7 cycle in ice-bath. Cell lysate is centrifuged at 14000 g for 10 minutes at 4 °C and the expressed protein is obtained in the supernatant.

Supernatant containing the expressed protein is purified using Nickel-Nitrilotriacetic acid beads (Qiagen), pre-previously equilibrated with lysis buffer. Beads are washed with four column volumes of buffer containing 50 mM potassium phosphate (pH 7), 250 mM NaCl and 1 mM PMSF and 30 mM imidazole to remove non-specific binding. The recombinant protein is eluted with buffer containing 50 mM potassium phosphate (pH 7), 250 mM NaCl and 1 mM PMSF and 250 mM imidazole.

Protein concentration ~6.2 μM is used in 12% Sodium dodecyl sulphate polyacrylamide gel electrophoresis (SDS-PAGE) to check the purity after affinity chromatography. Imidazole is removed from the sample by buffer exchange using a spin concentrator (10 KDa cut-off, Amicon) and lysis buffer. Concentration of pure protein is determined using Beer-Lambert law and absorbance 280 nm (BioSpectrometer, Eppendorf). Extinction coefficient (ε_{280}) from Protparam[51] tool (Expasy server) obtained for the construct sequence is 18450 $M^{-1}cm^{-1}$.

Mass Analysis. We perform mass spectrometry using MALDI-TOF Bruker Ultraflextreme spectrometer to determine the mass of purified protein. Protein is mixed in 1:1 ratio with sinapinic acid which is dissolved in a mixture of acetonitrile and trifluoroacetic acid (1:1).

Size Exclusion Chromatography.   The affinity chromatography purified protein is subjected to a size exclusion column (2.5×45 cm) packed with superdex75 (GE Healthcare) and equilibrated with lysis buffer. Protein concentration used for size exclusion chromatography is ~500 μM. Fractions of purified protein are eluted at a flow rate of 1 ml/min using a peristaltic pump (GE Healthcare). Absorbance at 280 nm wavelength is measured for all the fractions to identify the pure protein. Calibration of the column is performed using standard proteins namely, Lysozyme (14.4 KDa), Carbonic anhydrase (29 KDa), Ovalbumin (43 KDa), BSA (66 KDa) and Conalbumin (75 KDa). The error bars for standard proteins and STY3178 are estimated as standard errors from three sets of repeat experiments.

Circular Dichroism (CD).   CD measurements are performed in Jasco J-815 CD spectrometer at 20 °C using a quartz cuvette. In the absence and presence of antibiotics, far UV (200–250 nm) and near UV (250–330 nm) protein CD spectra are collected using 1 mm and 10 mm path-length cells, respectively. Concentration of protein used for far UV-CD is 10 μM and near UV-CD is 30 μM. Concentration of antibiotics used are: i) ciprofloxacin 5, 10, 20, 30 and 50 μM; ii) rifampin 10, 20, 50, 100 and 200 μM; iii) ampicillin 60, 200 and 300 μM. Isolated amino acid CD in presence of antibiotics is performed with 400 μM Tyr, 1000 μM Phe and 400 μM Trp. All measurements reported are an average of three scans and buffer subtracted.

Helical content of the protein is calculated using the following relation[25,26] $f_H = \frac{([\theta]_{222} - 3,000)}{(-36,000 - 3,000)}$, where f_H and $[\theta]_{222}$ are fractional helicity and mean residue ellipticity at 222 nm.

Dynamic Light Scattering (DLS).   The measurement is carried out in Nano-S Malvern instrument at 20 °C. Sample concentration of 10 μM is subjected to laser scattering of wavelength 632.8 nm where the measuring angle 173°. The hydrodynamic size of the protein-antibiotic complex is measured in presence of 50 μM ciprofloxacin, 200 μM rifampin and 200 μM ampicillin. Each measurement is obtained as a mean of five successive counts. All the samples prior to each measurement are passed through 0.22 μm syringe filter (Millipore).

Steady State Fluorescence Spectroscopy.   The spectra are recorded using Jobin Yvon Horiba Fluorolog with a slit width of 2 nm. Sample concentration of 10 μM is excited at wavelengths 257, 275, 280 and 295 nm. The final spectrum for each excitation wavelength is obtained after subtracting the lysis buffer spectrum. In presence of increasing concentration of antibiotics (ciprofloxacin, rifampin and ampicillin), the experiment is repeated in a similar way. Each data set represented is an averaged over two sets of measurements.

The fluorescence quenching data upon antibiotic binding to protein is analysed using Stern-Volmer equation[35–37], $(F_0 - F)/F = K_{SV}[Q]$ where F_0 and F, respectively, are the fluorescence intensities in absence and presence of the antibiotic at concentration Q and K_{SV} Stern-Volmer quenching constant. Using the modified form of Stern-Volmer equation[35–37], $\log[(F_0 - F)/F] = \log K + n \log[Q]$, value of binding constant (K) and the number of binding sites (n) are estimated along with dissociation constant (K_d) and ΔG using standard protocol[37].

Isothermal Titration Calorimetry (ITC).   ITC measurements are performed for STY3178 binding to ciprofloxacin, rifampin and ampicillin using MicroCal iTC200 calorimeter (GE healthcare). Pure protein is dialyzed against buffer containing 30 mM phosphate (pH7), 150 mM NaCl and 1 mM PMSF. Protein concentration used in the cell for these experiments is 300 μM. Antibiotics concentrations loaded in the syringe are 20 mM ciprofloxacin, 10 mM rifampin and 100 mM ampicillin. All titrations including protein- antibiotics and buffer- antibiotics are performed in dialysis buffer. Temperature and reference power used in ITC are 298 K and 10 μcal/s, respectively. A total of 30 injections with an initial delay of 60 sec for each antibiotic titration are performed with constant stirring at 50 rpm. First injection of 0.4 μl over a time period of 0.8 sec is followed by 29 injections of 0.6 μl each for 1.2 sec spaced by 200 sec between each injection. Integrated data after subtracting the heat of dilution for respective antibiotics are plotted using MicroCal origin. Rifampin data is fitted to single site binding model and ciprofloxacin and ampicillin data are fitted to sequential binding models to estimate K, enthalpy (ΔH) and entropy (ΔS). K_d is calculated from the reciprocal of K and change in free energy (ΔG) is estimated using Gibbs equation, $\Delta G = \Delta H - T\Delta S$.

NMR experiments.   STY3178 protein is uniformly ^{15}N-labeled using M9 minimal media supplemented with ^{15}NH$_4$Cl as a source of nitrogen. It is extracted and purified following the same protocol mentioned above in the purification section.

Relaxation measurements.   The one dimensional (1D) ^{1}H-^{15}N heteronuclear longitudinal (T_1) and transverse (T_2) relaxation experiments are performed at 30 °C using 600 MHz Varian spectrometer equipped with triple resonance probe. The final ^{15}N-labeled protein concentration used for the measurement is 355 μM in 30 mM phosphate buffer (pH 7), 150 mM NaCl and 10% D$_2$O. For T_1 measurement, d_1 time delays of 8, 9 and 12 s are used and that for T_2 measurement is 4 s. The free induction decay (FID) for T_1 is collected for the delay points 0.01, 0.05, 0.1, 0.2, 0.3, 0.4, 0.5, 0.6, 0.8, 1.0, 1.2, 1.5 and 1.8 s. Similarly, delays used for T_2 are 0.01, 0.03, 0.05, 0.07, 0.09, 0.11, 0.13, 0.15 and 0.17 s. All the FIDs are acquired for 256 scans. The data are processed using VnmrJ to obtain the intensity for the range 8.5–10.5 ppm for each set of delay. The intensities for all the d_1 time delays for both T_1 and T_2 data are first normalised for each individual data set and then averaged for all the data sets acquired at each delay point. The plot of intensity versus time is fitted to a single exponential function using SigmaPlot and T_1 and T_2 are calculated from the slope of the fitted curve. The total rotational correlation time (τ_C) is calculated using the equation[52,53] $\tau_C = \frac{1}{4\pi V_N}\sqrt{6\frac{T_1}{T_2} - 7}$ where V_N is nitrogen (^{15}N) resonance frequency in Hertz.

The τ_C estimations for the antibiotic bound protein are done in the same way as the native protein by measuring the T_1 and T_2 using NMR experiments for each bound case.

References

1. Bateman A., Coggill P. & Finn R. D. DUFs: families in search of function. *Acta Crystallogr, Sect F: Struct Biol Cryst Commun* **66,** 1148–1152 (2010).
2. Blattner F. R. *et al.* The complete genome sequence of Escherichia coli K-12. *Science* **277,** 1453–1462 (1997).
3. Parkhill J. *et al.* Complete genome sequence of a multiple drug resistant Salmonella enterica serovar Typhi CT18. *Nature* **413,** 848–852 (2001).
4. Fricke W. F. *et al.* Comparative Genomics of 28 Salmonella enterica Isolates: Evidence for CRISPR-Mediated Adaptive Sublineage Evolution. *Journal of Bacteriology* **193,** 3556–3568 (2011).
5. Deng W. *et al.* Comparative genomics of Salmonella enterica serovar Typhi strains Ty2 and CT18. *J Bacteriol* **185,** 2330–2337 (2003).
6. McClelland M. *et al.* Complete genome sequence of Salmonella enterica serovar typhimurium LT2. *Nature* **413,** 852–856 (2001).
7. Holt K. E. *et al.* Multidrug-resistant Salmonella enterica serovar Paratyphi A harbors IncHI1 plasmids similar to those found in serovar Typhi. *Journal of Bacteriology* **189,** 4257–4264 (2007).
8. Mulvey M. R., Boyd D., Cloeckaert A., Ahmed R. & Ng L. K. Emergence of multidrug-resistant Salmonella Paratyphi B dT + , Canada. *Emerg Infect Dis* **10,** 1307–1310 (2004).
9. Holt K. E. *et al.* Pseudogene accumulation in the evolutionary histories of Salmonella enterica serovars Paratyphi A and Typhi. *BMC Genomics* **10,** 36 (2009).
10. Jiang Y., Yu D., Wei Z., Shen P., Zhou Z. & Yu Y. Complete nucleotide sequence of Klebsiella pneumoniae multidrug resistance plasmid pKP048, carrying blaKPC-2, blaDHA-1, qnrB4, and armA. *Antimicrob Agents Chemother* **54,** 3967–3969 (2010).
11. Hirsch E. B. & Tam V. H. Detection and treatment options for Klebsiella pneumoniae carbapenemases (KPCs): an emerging cause of multidrug-resistant infection. *J Antimicrob Chemother* **65,** 1119–1125 (2010).
12. Nishino K. & Yamaguchi A. Overexpression of the response regulator evgA of the two-component signal transduction system modulates multidrug resistance conferred by multidrug resistance transporters. *J Bacteriol* **183,** 1455–1458 (2001).
13. Nishino K., Inazumi Y. & Yamaguchi A. Global analysis of genes regulated by EvgA of the two-component regulatory system in Escherichia coli. *J Bacteriol* **185,** 2667–2672 (2003).
14. Masuda N. & Church G. M. Escherichia coli gene expression responsive to levels of the response regulator EvgA. *J Bacteriol* **184,** 6225–6234 (2002).
15. Mullins E. A., Sullivan K. L. & Kappock T. J. Function and X-ray crystal structure of Escherichia coli YfdE. *PLoS One* **8,** e67901 (2013).
16. Parry C. M. *et al.* Randomized controlled comparison of ofloxacin, azithromycin and an ofloxacin-azithromycin combination for treatment of multidrug-resistant and nalidixic acid-resistant typhoid fever. *Antimicrob Agents Chemother* **51,** 819–825 (2007).
17. Rowe B., Ward L. R. & Threlfall E. J. Multidrug-resistant Salmonella typhi: a worldwide epidemic. *Clin Infect Dis* **24** Suppl 1, S106–109 (1997).
18. Kapil A., Sood S., Dash N. R., Das B. K. & Seth P. Ciprofloxacin in typhoid fever. *Lancet* **354,** 164 (1999).
19. Umasankar S., Wall R. A. & Berger J. A case of ciprofloxacin-resistant typhoid fever. *Commun Dis Rep CDR Rev* **2,** R139–140 (1992).
20. Senthilkumar B. & Prabakaran G. Multidrug resistant Salmonella typhi in asymptomatic typhoid carriers among food handlers in Namakkal district, Tamil Nadu. *Indian J Med Microbiol* **23,** 92–94 (2005).
21. Ellrott K. *et al.* TOPSAN: a dynamic web database for structural genomics. *Nucleic Acids Res* **39,** D494–496 (2011).
22. UniProt: a hub for protein information. *Nucleic Acids Res* **43,** D204–212 (2015).
23. Kanehisa M. & Goto S. KEGG: kyoto encyclopedia of genes and genomes. *Nucleic Acids Res* **28,** 27–30 (2000).
24. Franceschini A. *et al.* STRING v9.1: protein-protein interaction networks, with increased coverage and integration. *Nucleic Acids Res* **41,** D808–815 (2013).
25. Morrisett J. D., David J. S. K., Pownall H. J. & Gotto A. M. Jr. Interaction of an apolipoprotein (apoLP-alanine) with phosphatidylcholine. *Biochemistry* **12,** 1290–1299 (1973).
26. Correa D. H. A. & Ramos C. H. I. The use of Circular Dichroism spectroscopy to study protein folding, form and function. *Afr J Biochem Res* **3,** 164–173 (2009).
27. Whitmore L. & Wallace BA. DICHROWEB an online server for protein secondary structure analyses from circular dichroism spectroscopic data. *Nucleic Acids Res* **32,** W668–W673 (2004).
28. Lobley A., Whitmore L. & Wallace B. A. DICHROWEB: an interactive website for the analysis of protein secondary structure from circular dichroism spectra. *Bioinformatics* **18,** 211–212 (2002).
29. Whitmore L. & Wallace B. A. Protein secondary structure analyses from circular dichroism spectroscopy: methods and reference databases. *Biopolymers* **89,** 392–400 (2008).
30. Andrade M. A., Chacon P., Merelo J. J. & Moran F. Evaluation of Secondary Structure of Proteins from UV Circular-Dichroism Spectra Using an Unsupervised Learning Neural-Network. *Protein Eng* **6,** 383–390 (1993).
31. Claes P. D. M., Kenney A. & Vardy P. An on-line dynamic light scattering instrument for macromolecular characterization in *Laser* Light *scattering in biochemistry*. (eds S. E. Harding, D. B. Sattelle and V. A. Bloomfield) 66–76 (1992).
32. Hereld D., Krakow J. L., Bangs J. D., Hart G. W. & Englund P. T. A phospholipase C from Trypanosoma brucei which selectively cleaves the glycolipid on the variant surface glycoprotein. *J Biol Chem* **261,** 13813–13819 (1986).
33. Blake-Hodek K. A., Cassimeris L. & Huffaker T. C. Regulation of microtubule dynamics by Bim1 and Bik1, the budding yeast members of the EB1 and CLIP-170 families of plus-end tracking proteins. *Mol Biol Cell* **21,** 2013–2023 (2010).
34. Van-Quynh A., Willson S. & Bryant R. G. Protein reorientation and bound water molecules measured by H-1 magnetic spin-lattice relaxation. *Biophysical Journal* **84,** 558–563 (2003).
35. Lakowicz J. R. In *Principles of Fluorescence Spectroscopy* 3rd edn, Ch. 8, 277–290 (Springer, 2006).
36. Patel S. & Datta A. Steady state and time-resolved fluorescence investigation of the specific binding of two chlorin derivatives with human serum albumin. *J Phys Chem B* **111,** 10557–10562 (2007).
37. Anand U., Kurup L. & Mukherjee S. Deciphering the role of pH in the binding of ciprofloxacin hydrochloride to bovine serum albumin. *Phys Chem Chem Phys* **14,** 4250–4258 (2012).
38. Kelly S. M., Jess T. J. & Price N. C. How to study proteins by circular dichroism. *Bba-Proteins Proteom* **1751,** 119–139 (2005).
39. Sun Y. & MacRae T. H. Small heat shock proteins: molecular structure and chaperone function. *Cell Mol Life Sci* **62,** 2460–2476 (2005).
40. Bachas S., Eginton C., Gunio D. & Wade H. Structural contributions to multidrug recognition in the multidrug resistance (MDR) gene regulator, BmrR. *Proc Natl Acad Sci USA* **108,** 11046–11051 (2011).
41. Nakashima R., Sakurai K., Yamasaki S., Nishino K. & Yamaguchi A. Structures of the multidrug exporter AcrB reveal a proximal multisite drug-binding pocket. *Nature* **480,** 565–569 (2011).
42. Ziervogel B. K. & Roux B. The binding of antibiotics in OmpF porin. *Structure* **21,** 76–87 (2013).
43. Yamasaki S. *et al.* The crystal structure of multidrug-resistance regulator RamR with multiple drugs. *Nat Commun* **4,** 2078 (2013).
44. Lewis K. Multidrug resistance: Versatile drug sensors of bacterial cells. *Curr Biol* **9,** R403–407 (1999).

45. Sikora C. W. & Turner R. J. SMR proteins SugE and EmrE bind ligand with similar affinity and stoichiometry. *Biochem Biophys Res Commun* **335,** 105–111 (2005).

46. Sikora C. W. & Turner R. J. Investigation of ligand binding to the multidrug resistance protein EmrE by isothermal titration calorimetry. *Biophys J* **88,** 475–482 (2005).

47. Long F., Rouquette-Loughlin C., Shafer W. M. & Yu E. W. Functional cloning and characterization of the multidrug efflux pumps NorM from Neisseria gonorrhoeae and YdhE from Escherichia coli. *Antimicrob Agents Chemother* **52,** 3052–3060 (2008).

48. Kamat B. P. & Seetharamappa J. Mechanism of interaction of vincristine sulphate and rifampicin with bovine serum albumin: A spectroscopic study. *J Chem Sci* **117,** 649–655 (2005).

49. Mihaela Bacalum H. W. & M. Radu. Interaction between ceftazidime and bacterial porin OmpF analyzed by fluorescence. *Romanian Journal of Biophysics* **19,** 105–116 (2009).

50. Altschul S. F., Gish W., Miller W., Myers E. W. & Lipman D. J. Basic local alignment search tool. *J Mol Biol* **215,** 403–410 (1990).

51. Gasteiger E. *et al.* Protein Identification and Analysis Tools on the ExPASy Server; (In) *John M Walker (ed): The Proteomics Protocols Handbook*, Humana Press, 571–607 (2005).

52. Kay L. E., Torchia D. A. & Bax A. Backbone dynamics of proteins as studied by 15N inverse detected heteronuclear NMR spectroscopy: application to staphylococcal nuclease. *Biochemistry* **28,** 8972–8979 (1989).

53. Farrow N. A. *et al.* Backbone dynamics of a free and phosphopeptide-complexed Src homology 2 domain studied by 15N NMR relaxation. *Biochemistry* **33,** 5984–6003 (1994).

Acknowledgements

Author Contributions

MG planned the research. PS carried out the experiments. CM helped in sample preparation and ITC measurements. SD provided the initial laboratory support for experiments. MG, PS and SD analysed the results. MG and PS wrote the paper. All authors reviewed the manuscript.

Additional Information

Supplementary information accompanies this paper at http://www.nature.com/srep

Competing financial interests: The authors declare no competing financial interests.

How to cite this article: Saha, P. *et al.* Antibiotic binding of STY3178, a yfdX protein from *Salmonella* Typhi. *Sci. Rep.* **6**, 21305; doi: 10.1038/srep21305 (2016).